Estimates of turbulent diffusivities and energy dissipation rates from satellite measurements of spectra of stratospheric...

1 author:

Nikolai M. Gavrilov
Saint Petersburg State University
223 PUBLICATIONS **1,082** CITATIONS

Estimates of turbulent diffusivities and energy dissipation rates from satellite measurements of spectra of stratospheric refractivity perturbations

N. M. Gavrilov

Atmospheric Physics Department, Saint-Petersburg State University, St. Petersburg, Russia

Correspondence to: N. M. Gavrilov (gavrilov@pobox.spbu.ru)

Abstract. Approaches for estimations of effective turbulent diffusion and energetic parameters from characteristics of anisotropic and isotropic spectra of perturbations of atmospheric refractivity, density and temperature are developed. The approaches are applied to the data obtained with the GOMOS instrument for measurements of stellar scintillations on-board the Envisat satellite to estimate turbulent Thorpe scales, L_T, diffusivities, K, and energy dissipation rates, ε, in the stratosphere. At low latitudes, effective values are $L_T \sim$ 1–1.1 m, $\varepsilon \sim (1.8–2.4) \times 10^{-5}\,\mathrm{W\,kg^{-1}}$, and $K \sim (1.2–1.6) \times 10^{-2}\,\mathrm{m^2\,s^{-1}}$ at altitudes of 30–45 km in September–November 2004, depending on different assumed values of parameters of anisotropic and isotropic spectra. Respective standard deviations of individual values, including all kinds of variability, are $\delta L_T \sim 0.6–0.7\,\mathrm{m}$, $\delta\varepsilon \sim (2.3–3.5) \times 10^{-5}\,\mathrm{W\,kg^{-1}}$, and $\delta K \sim (1.7–2.6) \times 10^{-2}\,\mathrm{m^2\,s^{-1}}$. These values correspond to high-resolution balloon measurements of turbulent characteristics in the stratosphere, and to previous satellite stellar scintillation measurements. Distributions of turbulent characteristics at altitudes of 30–45 km in low latitudes have maxima at longitudes corresponding to regions of increased gravity wave dissipation over locations of stronger convection. Correlations between parameters of anisotropic and isotropic spectra are evaluated.

1 Introduction

Internal gravity waves (IGWs) with energy propagating upwards are important for dynamical processes and mixing in the middle atmosphere (Fritts and Alexander, 2003). Breaking IGWs produce turbulent mixing and kinetic energy dissipation and effectively influence the global circulation and composition in the middle atmosphere.

IGW studies use different in situ, ground-based and satellite measurements (Fritts and Alexander, 2003; Wu et al., 2006; Alexander et al., 2010). Key advantages of satellite measurements are their global coverage. To examine atmospheric mesoscale variations, Fetzer and Gille (1994) used satellite data of LIMS (Limb Infrared Monitor of the Stratosphere). Eckermann and Preusse (1999) presented the results of data processing of the satellite CRISTA (Cryogenic Infrared Spectrometer and Telescopes for the atmosphere) experiment. Wu and Waters (1996) and McLandress et al. (2000) studied mesoscale temperature perturbations and obtained their global distribution in the stratosphere and mesosphere from the data of MLS (Microwave Limb Sounder) instrument on-board the satellite UARS. Extensive information on atmospheric mesoscale fluctuations were given by the GPS/Microlab satellite (Tsuda et al., 2000; Alexander et al., 2002; Gavrilov et al., 2004; Gavrilov and Karpova, 2004). Studies of mesoscale variations using a GPS radio occultation technique were continued with satellite CHAMP launched in April 2001, and later with COSMIC group of satellites launched in 2006 (Schmidt et al., 2008; Alexander et al., 2008; Wang and Alexander, 2010). Ern et al. (2004, 2011) obtained global distributions of IGW momentum fluxes in the middle atmosphere from

global temperature measurements with the satellite instruments High Resolution Dynamics Limb Sounder (HIRDLS) and Sounding of the Atmosphere using Broadband Emission Radiometry (SABER).

Recent observations of stellar scintillations from satellites (Gurvich and Kan, 2003a, b; Sofieva et al., 2007, 2009, 2010) provided new information about small-scale perturbations in the stratosphere. The intensity of stellar light going through the atmosphere fluctuates (oscillates), when a satellite observes a star. Relative intensity fluctuations can be as strong as several hundred percent (see Sofieva et al., 2010). These scintillations are due to air temperature and density irregularities produced by IGWs, turbulence and different instabilities, which produce perturbations of atmospheric refractivity. The smallest scales measurable by an optical scintillation method may be less than a meter. Scintillation measurements provide information about IGW-breaking and turbulence in the stratosphere.

First measurements of stellar scintillations with the Russian space stations Salyut and Mir provided spectral and statistical characteristics of perturbations (Gurvich et al., 2001), and also confirmed the theory of scintillations (Gurvich and Brekhovskikh, 2001). These measurements also allowed determinations of IGW and turbulence spectra characteristics (Gurvich and Kan, 2003a, b; Gurvich and Chunchuzov, 2003).

Multi-year measurements were performed with the Global Ozone Monitoring by Occultation of Stars (GOMOS) instrument from the Envisat satellite (Bertaux et al., 2010). GOMOS contains two photometers recording stellar light at a sampling frequency of 1 kHz synchronously in 473–527 nm and 646–698 nm spectral bands during star sets behind the Earth's limb. These measurements were used to estimate parameters of anisotropic and isotropic spectra of temperature perturbations produced by IGWs and small-scale turbulence in the stratosphere (Gurvich and Kan, 2003a; Sofieva et al., 2007, 2009, 2010).

In this paper, we developed approaches to use these spectral parameters for estimating turbulent kinetic energy dissipation rates and turbulent diffusivities produced by small-scale isotropic turbulence. We estimated the mentioned turbulent characteristics at altitudes of 30–45 km in September–November 2004 at latitudes 20° S–20° N and in January 2005 at middle latitudes 34–36° N and compared them with available satellite, balloon and high-resolution radiosonde data.

2   Atmospheric perturbation spectra

Sofieva et al. (2007, 2009) estimated scales of isotropic and anisotropic parts of atmospheric perturbation spectra using observations of stellar scintillations with the GOMOS instrument on-board the Envisat satellite. Scintillations produced by density perturbations along the light path give information about small-scale atmospheric dynamics (Tatarskii,

1971). Sofieva et al. (2007, 2009) considered structures of relative fluctuations $\nu = N_r' / \overline{N_r} \approx -T' / \overline{T}$ of refractivity N_r and temperature T (overbars and primes denote the statistical means and perturbations, respectively). These structures could be described with the three-dimensional spectral density function $\Phi_\nu(\boldsymbol{k})$, where $\boldsymbol{k}$ is the wave vector with components $(\boldsymbol{k}_x, \boldsymbol{k}_y, \boldsymbol{k}_z)$ along horizontal axes x, y and vertical axis z, respectively. Gurvich and Kan (2003a) and Sofieva et al. (2007) approximated Φ_ν with a sum

$$\Phi_\nu = \Phi_W + \Phi_K, \tag{1}$$

where Φ_W and Φ_K are statistically independent anisotropic and isotropic components, respectively. The component Φ_W corresponds to anisotropic perturbations, produced, for example, by random IGWs (Smith et al., 1987). Gurvich and Kan (2003a) and Sofieva et al. (2007) approximated this three-dimensional spectrum as

$$\Phi_W(k_a) = C_W \eta^2 (k_a^2 + k_0^2)^{-5/2} \phi(k_a / k_W), \tag{2}$$
$$k_a^2 = \eta^2 k_h^2 + k_z^2; k_h^2 = k_x^2 + k_y^2,$$

where C_W and k_0 are parameters, η is the anisotropy coefficient, and the function $\phi(k / k_W)$ describes the decay of Φ_W at $k > k_W$. Integration of Eq. (2) gives the one-dimensional vertical spectrum $V_W(k_z)$:

$$V_W(k_z) = \int\limits_{-\infty}^{\infty} \int\limits_{-\infty}^{\infty} \Phi_W(k_a) dk_x dk_y \approx \frac{2\pi}{3} C_W (k_z^2 + k_0^2)^{-3/2}. \tag{3}$$

This expression does not depend on the anisotropy coefficient η. At $k_z \gg k_0$ the spectrum (Eq. 3) corresponds to the k_z^{-3} slope known for saturated IGWs (Smith et al., 1987). As far as $V_W(-k_z) = V_W(k_z)$, one can use the symmetric one-dimension spectrum, (see Monin and Yaglom, 1975, §12)

$$E_W(|k_z|) = 2V_W(k_z) = \frac{4\pi}{3} C_W (k_z^2 + k_0^2)^{-3/2}. \tag{4}$$

The second component, Φ_K, in Eq. (1) corresponds to isotropic turbulent irregularities produced by breaking IGWs and by other sources. Gurvich and Kan (2003a) and Sofieva et al. (2007) used a theory of locally isotropic turbulence, which gives

$$\Phi_K(k) = 0.033 C_K k^{-11/3} \exp[-(k / k_K)^2]; k^2 = k_h^2 + k_z^2, \tag{5}$$

where k_K is a parameter, C_K is the structure characteristic of the random refractivity field (see Monin and Yaglom, 1975, §23). The isotropic one-dimension spectrum $E_K(|k_z|)$ can be obtained by integration of the locally isotropic spectrum Φ_K (see Monin and Yaglom. 1975, §21), and at $|k_z| \ll k_K$ has the following form:

$$E_K(|k_z|) \approx 0.25 C_K |k_z|^{-5/3}, \tag{6}$$

which corresponds to the known −5/3 power law for Kolmogorov's turbulence (see Monin and Yaglom, 1975, §21).

The structure function $D_T(r)$ of the locally isotropic temperature field at displacements r (Tatarskii, 1971) has the form

$$D_T(r) = \overline{[T(z+r) - T(z)]^2} = C_T^2 r^{2/3}, \tag{7}$$

where C_T^2 is the structure characteristic of the temperature field. According to Monin and Yaglom (1975, §13.3) for locally isotropic turbulence

$$D_T(r) = 2 \int_0^\infty (1 - \cos k'r) E_K(k') dk' = C_K \bar{T}^2 r^{2/3}. \tag{8}$$

Comparing in Eqs. (7) and (8), one can get

$$C_K = C_T^2 / \bar{T}^2. \tag{9}$$

Sofieva et al. (2007, 2009) developed algorithms for estimating the four parameters of anisotropic and isotropic spectra (Eqs. 2–6): the structure characteristics C_K and C_W, and wavenumbers k_W and k_0, which correspond to inner and outer scales of the anisotropic spectrum (Eq. 2). These algorithms were used to obtain these four parameters from observations of stellar scintillations with the GOMOS instrument on-board the Envisat satellite (Sofieva et al., 2007, 2009).

3 Estimation of turbulence characteristics

In Sect. 3.1 below, we obtain formulae connecting turbulent energy dissipation rates, diffusivities and other turbulent characteristics with parameters of anisotropic and isotropic parts of atmospheric perturbation spectra (Eqs. 4, 6). We use these formulae for estimations of turbulent characteristics in the stratosphere from GOMOS satellite data in Sect. 3.2. Possible correlations between anisotropic and isotropic spectral parameters are considered in Sect. 3.3.

3.1 Relations between turbulent and spectral characteristics

Some theories of turbulent spectra (for example, Lumley, 1964) introduce the "buoyancy" wavenumber k_b for the crossover between vertical anisotropic (Eq. 4) and isotropic (Eq. 6) spectral regimes, $E_W(k_b) = E_K(k_b)$ so that

$$k_b \approx (16.8 C_W / C_K)^{3/4}. \tag{10}$$

This parameter could be a useful addition to the discussed above parameters of anisotropic (C_W, k_0, k_W) and isotropic (C_K) parts of refractivity perturbation spectra (Eqs. 1–6). Figure 1 shows an example of vertical anisotropic (Eq. 4) and isotropic (Eq. 6) components of the temperature perturbation spectrum (Eq. 1) and the above-mentioned scales. The buoyancy wavenumber k_b, as well as k_W, correspond to a transition from anisotropic to isotropic perturbation spectra,
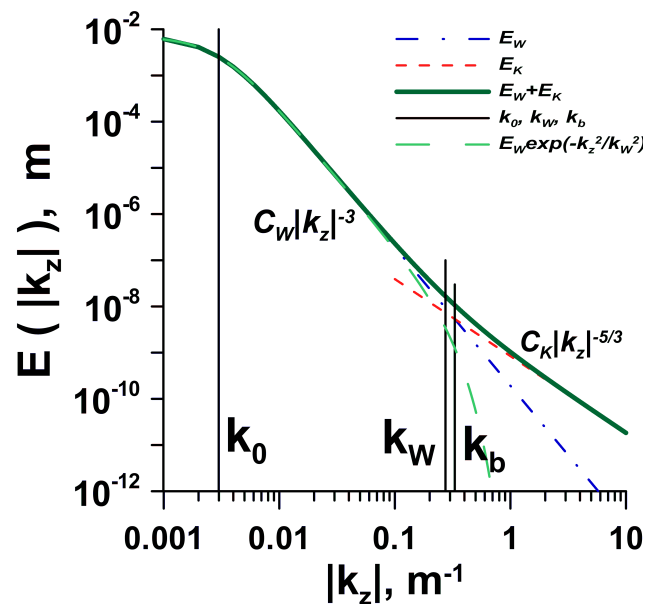

Fig. 1. One-dimension anisotropic (Eq. 4) and isotropic (Eq. 6) components of temperature perturbation spectrum (Eq. 1) for average parameters at altitudes of 30–45 km given in Table 1.

which we denote as a wavenumber k_m below. An important characteristic of turbulence in stably stratified layers is the Thorpe length $L_T = [\overline{\theta'^2}/(\partial\bar{\theta}/\partial z)^2]^{1/2}$, where θ is potential temperature (see Gavrilov et al., 2005). The contribution to the relative temperature variance produced by turbulent perturbations having $|k_z| \geq k_m$ can be calculated by integrating the isotropic spectrum (Eq. 6) as follows:

$$\frac{\overline{T'^2}}{\bar{T}^2} = \int_{k_m}^\infty E_K(k') dk' = 0.37 C_K k_m^{-2/3}. \tag{11}$$

Taking account of $\theta'/\bar{\theta} \approx T'/\bar{T}$ (see Tatarskii, 1971) and using (Eq. 11), one can get the following expression for the Thorpe scale:

$$L_{Tm} \approx \frac{g(0.37 C_K k_m^{-2/3})^{1/2}}{N^2}; \quad N^2 = \frac{g}{\theta} \frac{\partial\bar{\theta}}{\partial z}. \tag{12}$$

A similar expression was obtained by Gavrilov et al. (2005). To estimate L_T, one can also use the expression based on the consideration of turbulent energy balance by Ottersten (1969) with the hypotheses of incompressibility and isotropic and stationary turbulence (see Gavrilov et al. 2005), which, taking account of Eqs. (6)–(8), has the form

$$L_{Te} = (0.88 C_K g^2)^{3/4} / N^3. \tag{13}$$

This formula contains the only one parameter C_K of the isotropic perturbation spectrum (Eq. 4). Gavrilov et al. (2005) obtained reasonable agreement between (Eq. 13)

and direct measurements of L_T from the data of high-resolution MUTSI balloon measurements in the troposphere and stratosphere. For steady-state turbulence, energy dissipation rate, ε, and turbulent diffusivity, K, are related to the Ozmidov scale, L_O, by

$$\varepsilon \approx L_O^2 N^3; \quad K \approx \beta L_O^2 N, \tag{14}$$

where β is a constant. According to a review by Fukao et al. (1994), β may vary between 0.2 and 1. The frequently used approximation $\beta = Rf/(1-Rf)$, where Rf is the flux Richardson number, often taken as $Rf \approx 0.25$, gives $\beta \approx 1/3$. Assuming $L_O = cL_T$, Caldwell (1983), and more recently, Galbraith and Kelley (1996), also Fer et al. (2004) proposed the following formulae for estimations of ε and K:

$$\varepsilon \approx (cL_T)^2 N^3; \quad K \approx \beta(cL_T)^2 N. \tag{15}$$

Values of the empirical constant c vary in different studies (see discussions by Gavrilov et al., 2005 and Clayson and Kantha, 2008). After Gavrilov et al. (2005), considering the result given by Alisse (1999) for stratospheric data, we below use $c = 1.15$ and $\beta = 1/3$. Formulae Eqs. (15) and (10), (12) or (13) one can use for estimations of L_T, ε and K depending on a set of spectral parameters available experimentally. In the case of GOMOS scintillation observations, we have the entire set of parameters C_W, k_0, k_W and C_K, which is enough for the usage of any combinations of formulae (Eqs. 10–15). This allows us to compare the results obtained with different approaches using Eqs. (15) and (10), (12) or (13) in the next section.

3.2 Turbulent diffusivities and energy dissipation rates

The methods of estimating the parameters C_W, k_0, k_W of anisotropic (Eq. 2) and C_K of isotropic (Eq. 5) spectra of atmospheric temperature perturbations from GOMOS satellite observations of star scintillations were described by Sofieva et al. (2007, 2009, 2010). The retrieval uses the standard maximum-likelihood method with a combination of nonlinear and linear optimization. The authors made nonlinear fits of two parameters k_0 and k_W using the Levenberg–Marquardt algorithm (Press et al., 1992). The parameters C_K and C_W were calculated with the linear weighted least-squares method. Atmospheric parameters required for the spectral parameter retrievals are taken from the ECMWF meteorological reanalysis model. Sofieva et al. (2007, 2009, 2010) presented examples of the experimental scintillation spectrums. Usually, experimental scintillations agree to the proposed modeled scintillation spectra, but sometimes peaks, possibly related to quasi-periodic disturbances in the atmosphere, may occur and special filtering of these peaks was applied by Sofieva et al. (2007, 2009, 2010).

In the present paper, we use two sets of four parameters C_W, k_0, C_K and k_W from GOMOS scintillation measurements by Sofieva et al. (2007, 2009, 2010). The first set includes data obtained for occultations of the brightest stars

Sirius and Canopus in September–November 2004 at latitudes between 20° N and 20° S, which give the highest signal to noise ratios. We selected four groups of measurements at altitudes within 3 km-thick layers centered at 30, 35, 40 and 45 km altitudes. The second set of analyzed data is the Canopus occultations for January 2005 at 30 km altitude and latitudes 34–36° N, which allows comparisons with high-resolution radiosonde turbulence measurements by Clayson and Kantha (2008). The method by Sofieva et al. (2007, 2009, 2010) also gives estimations of errors of the spectral parameters. In the present study, we used values of spectral parameters having relative errors smaller than 50 %. Table 1 shows the numbers of measurements n used in our analysis in each altitude layer and data set.

For each set of measured parameters C_W and C_K, using Eq. (10), we estimated the buoyancy wavenumber k_b. The Thorpe scales L_{Tb} and L_{TW} are obtained from Eq. (12) putting $k_m = k_b$ and $k_m = k_W$, respectively, as well as the Thorpe scale L_{Te} from Eq. (13). Then, Eq. (15) gives values of the turbulent energy dissipation rates ε_b, ε_W, ε_e and turbulent diffusivities K_b, K_W, K_e, after substitutions of $L_T = L_{Tb}$, L_{TW}, L_{Te}, respectively. Table 1 gives average values and standard deviations of spectral scales and turbulence characteristics for all used sets of experimental data. To increase numbers of measurements for statistical comparisons of different approaches used for estimating turbulent characteristics, Table 1 includes results obtained for combined altitude range of 30–45 km in September–November 2004. Standard deviations shown in Table 1 take into account all kinds of variability (time, latitude, longitude and altitude) of individual values. Considering Table 1, one should keep in mind that if atmospheric turbulence differs from locally homogeneous and isotropic conditions, estimations of spectral scales from GOMOS data and our estimations of turbulent parameters should be considered as some "effective" values only.

Because of the large spatial and temporal variability of the turbulent parameters, their statistical distributions could be more informative than just averages and standard dispersions. Figure 2 presents histograms of the spectral parameters and turbulence characteristics for September–November 2004 at 40 km altitude. Respective histograms for other heights layers have forms similar to Fig. 2, and their parameters are given in Table 1. All histograms in Fig. 2 have strongly non-Gaussian shapes.

For January 2005 Table 1 gives estimations of the average Thorpe scales by different approaches in the range $L_T \sim 0.34$–0.44 m at 30 km altitude at latitudes 34–36° N. Respective average turbulent energy dissipation rates in Table 1 are $\varepsilon \sim (1.8$–$2.9) \times 10^{-6}$ W kg^{-1} and turbulent diffusivities $K \sim (1.3$–$2.0) \times 10^{-3}$ m^{2}s^{-1}. Dispersions in these estimations are caused by usage of different $k_m = k_b$ and $k_m = k_W$ in Eq. (12) for calculation of L_{Tb} and L_{TW} and usage of Eq. (13) to calculate L_{Te}, also by possible uncertainties in semi-empirical coefficients in these formulae.

Table 1. Averages and standard deviations of the spectral parameters and turbulence characteristics.

Year	2004	2004	2004	2004	2004	2005
Months	9–11	9–11	9–11	9–11	9–11	1
z, km	30	35	40	45	30–45	30
Latitudes, DEG	20° S–20° N	20° S–20° N	20° S–20° N	20° S–20° N	20° S–20° N	34° N–36° N
n	594	596	597	587	2374	147
N^2, $10^{-4}\,\mathrm{s}^{-2}$	5.13 ± 0.29	5.11 ± 0.51	5.01 ± 0.38	4.36 ± 0.37	4.80 ± 0.51	4.94 ± 0.48
C_W, $10^{-11}\,\mathrm{m}^{-2}$	3.78 ± 1.08	4.26 ± 1.63	5.71 ± 2.55	4.51 ± 2.42	4.57 ± 2.19	4.52 ± 1.39
k_0, $10^{-3}\,\mathrm{m}^{-1}$	4.02 ± 3.31	3.43 ± 3.25	2.75 ± 3.30	1.77 ± 1.99	2.99 ± 3.13	5.34 ± 3.32
C_K, $10^{-9}\,\mathrm{m}^{-2/3}$	1.36 ± 0.74	3.37 ± 1.55	5.72 ± 3.68	3.02 ± 2.65	3.37 ± 2.91	0.80 ± 0.32
k_W, m^{-1}	0.41 ± 0.09	0.34 ± 0.10	0.22 ± 0.08	0.13 ± 0.06	0.27 ± 0.14	0.47 ± 0.09
k_b, m^{-1}	0.62 ± 0.19	0.34 ± 0.12	0.34 ± 0.20	0.48 ± 0.28	0.44 ± 0.23	1.04 ± 0.30
L_{Tb}, m	0.51 ± 0.19	1.00 ± 0.35	1.37 ± 0.66	1.01 ± 0.59	0.98 ± 0.58	0.34 ± 0.10
L_{TW}, m	0.57 ± 0.15	0.98 ± 0.26	1.47 ± 0.55	1.41 ± 0.63	1.11 ± 0.59	0.44 ± 0.11
L_{Te}, m	0.53 ± 0.20	1.07 ± 0.42	1.60 ± 0.82	1.19 ± 0.75	1.10 ± 0.72	0.38 ± 0.13
ε_b, $10^{-5}\,\mathrm{W\,kg}^{-1}$	0.46 ± 0.46	1.66 ± 1.10	3.37 ± 3.11	1.64 ± 2.24	1.78 ± 2.32	0.18 ± 0.10
ε_W, $10^{-5}\,\mathrm{W\,kg}^{-1}$	0.53 ± 0.30	1.52 ± 0.74	3.58 ± 2.62	2.83 ± 3.72	2.11 ± 2.90	0.29 ± 0.13
ε_e, $10^{-5}\,\mathrm{W\,kg}^{-1}$	0.49 ± 0.48	1.92 ± 1.46	4.66 ± 4.45	2.33 ± 3.81	2.35 ± 3.54	0.23 ± 0.14
K_b, $10^{-2}\,\mathrm{m}^2\mathrm{s}^{-1}$	0.30 ± 0.30	1.10 ± 0.78	2.28 ± 2.12	1.26 ± 1.75	1.24 ± 1.65	0.13 ± 0.07
K_W, $10^{-2}\,\mathrm{m}^2\mathrm{s}^{-1}$	0.34 ± 0.20	1.01 ± 0.52	2.42 ± 1.81	2.18 ± 2.99	1.49 ± 2.24	0.20 ± 0.09
K_e, $10^{-2}\,\mathrm{m}^2\mathrm{s}^{-1}$	0.32 ± 0.32	1.29 ± 1.08	3.16 ± 3.08	1.79 ± 3.06	1.64 ± 2.62	0.16 ± 0.10

Clayson and Kantha (2008) estimated turbulent characteristics in 2005 at middle latitudes 30–39° N and longitudes 84–104° W from high-resolution radiosonde data. At altitudes of about 25 km they found average values of $L_T < 1$ m, $\varepsilon \sim 10^{-6}$–$10^{-5}\,\mathrm{W\,kg}^{-1}$ and $K < 10^{-2}\,\mathrm{m}^2\,\mathrm{s}^{-1}$, which are consistent with average turbulent characteristics for January 2005 presented in Table 1. Because our GOMOS data are just for January 2005, for higher altitude (30 km) and for entire longitudinal circle, further comparisons with balloon and radiosonde turbulence measurements that are better collocated in time and space are required.

Consideration of Table 1 for September–November 2004 shows monotonic decrease in stability and average N^2 values from 30 km to 45 km altitude at low latitudes. Average characteristic wavenumbers k_0 and k_W of the anisotropic spectrum (Eq. 2) also decrease in height in Table 1, while parameters C_W and C_K in Eqs. (2) and (5) have maxima at 40 km altitude. Estimated average buoyancy wavenumbers k_b in Table 1 are generally larger than wavenumbers of anisotropic spectrum decrease k_W (see also Fig. 1). Estimates of Thorpe scales L_{TW} and L_{Te} averaged over altitudes of 30–45 km are quite close in Table 1, while average L_{Tb} is little bit smaller. At particular altitudes in Table 1, differences between L_{Tb}, L_{TW} and L_{Te} are larger and could be partly caused by uncertainties in semi-empirical constants in Eqs. (12) and (13). Relative differences between maximum and minimum values ε_b, ε_W, ε_e do not exceed 30–50 % at different altitudes in Table 1, and respectively, K_b, K_W, K_e do not differ more than 20–40 %.

Figure 3 shows a comparison of latitude-longitude distributions of different estimates of turbulent energy dissipation

rates in September–November 2004 at 40 km altitude. One can see similar distributions of all estimates ε_b, ε_W and ε_e, although values of ε_e are generally larger in Fig. 3. According to Table 1, the differences between averages of ε_b, ε_W and ε_e could be smaller at other altitudes, than that at 40 km altitude in September–November 2004. Therefore, all expressions (Eq. 12) with $k_m = k_b$ and $k_m = k_W$, as well as Eq. (13) can be used for estimations of distributions of Thorpe scales and subsequent estimations of turbulent energy dissipation rates and turbulent diffusivities (Eq. 15), depending on spectral parameters available from experiments.

Figure 4 shows latitude-longitude distributions of turbulent diffusivity estimate K_W in September–November 2004 at different altitudes. One can see substantial variability of these distributions in altitude. Latitude-longitude distributions similar to Fig. 4 were obtained for C_K and other estimates of turbulent diffusivity and turbulent energy dissipation rate. Although maxima of K_W are concentrated at the same longitudes as C_K maxima in Fig. 3, their distributions may vary at different altitudes in Fig. 4.

3.3 Correlations between spectral parameters.

Parameters C_W, k_0, k_W of anisotropic (Eq. 2) and C_K of isotropic (Eq. 5) spectra may be related to each other. For example, increasing small-scale isotropic turbulence can cause increased dissipation of larger scale anisotropic motions in the atmosphere, also instabilities of anisotropic motions can cause generation of increased isotropic turbulence. At numbers of recorded values $n > 580$ at different altitudes for September–November 2004 in Table 1, the hypothesis about
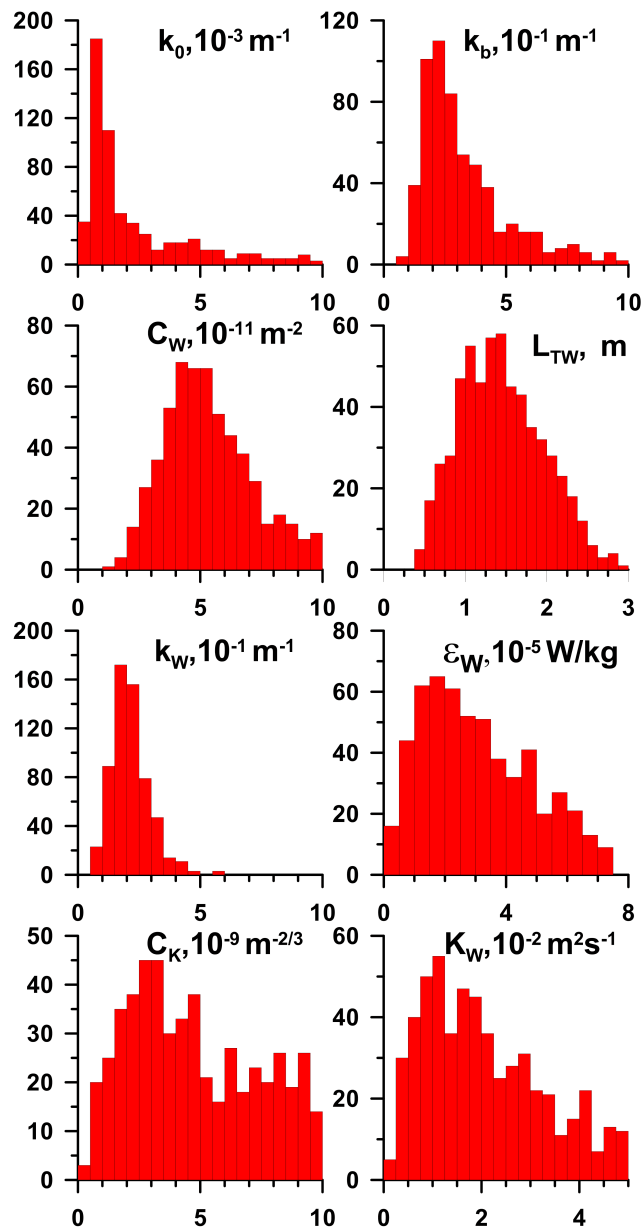
Fig. 2. Histograms of anisotropic and isotropic spectral parameters and turbulent characteristics in September–November 2004 at 40 km altitude.

Fig. 3. Latitude-longitude distributions of different estimates of turbulent energy dissipation rates in September–November 2004 at 40 km altitude.

of turbulent characteristics, their local values can be substantially different from those effective values.

Figure 5 shows scatter plots for pairs of spectral parameters presented in Table 2 for September–November 2004 at 40 km altitude. Dependences between these parameters in Fig. 5 can be approximated with power laws $y = aC_W^\gamma$, where y represents any of quantities C_K, k_0, or k_W. Corresponding power law parameters a and γ for these quantities, obtained with least-square fitting (in logarithmic coordinates) at different altitudes, are given in Table 2.

4 Discussion

Average values of different Thorpe scales L_{Ti} are about, or smaller than 1 m in Table 1 at altitudes of 30–35 km. Respective average turbulent energy dissipation rates are $\varepsilon_i \leq 2 \times 10^{-5}\,\mathrm{W\,kg^{-1}}$ and turbulent diffusivities $K_i \leq 1.3 \times 10^{-2}\,\mathrm{m^2\,s^{-1}}$. Gavrilov et al. (2005) obtained the same orders of magnitude for these quantities from the analysis of high-resolution temperature profiles obtained during the MUTSI campaign. High-resolution radiosonde measurements by Clayson and Kantha (2008) also gave average

nonzero linear dependence between two variables has confidence > 0.999 when the absolute values of cross-correlation coefficients between them are $|r| > 0.1$ (see Press et al., 1992). Table 2 shows cases, when $|r|$ were larger 0.1 and r had the same signs at all altitudes for data sets presented in Table 1. One can see that the largest positive correlations exist between parameters C_W and C_K. Smaller positive correlations exist between C_W and k_0 and negative correlation between C_W and k_W in Table 2. One should keep in mind that the regressions shown in Table 2 represent some effective values of respective parameters. Due to big dispersions
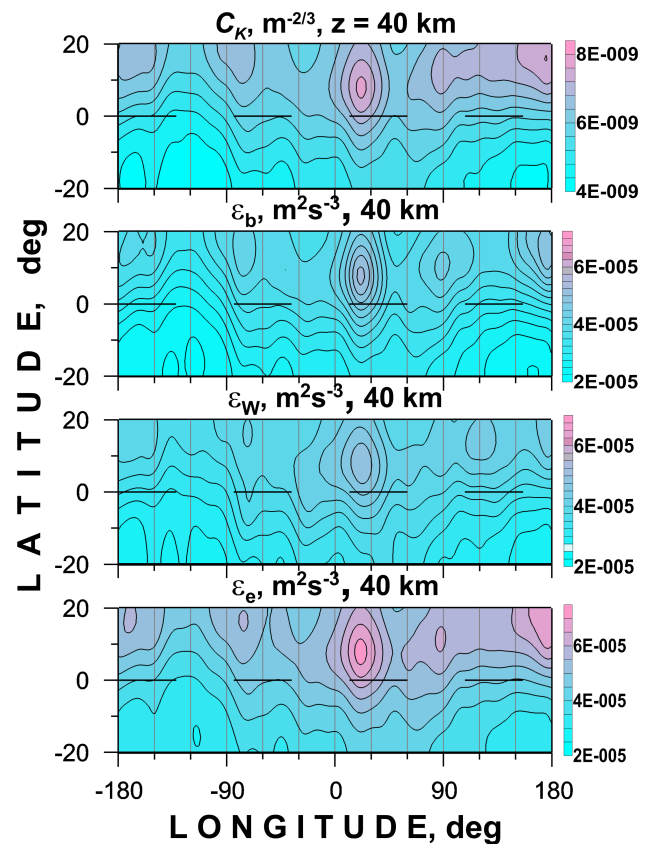
Table 2. Cross-correlation coefficients and parameters of power dependences between parameters of anisotropic and isotropic components of atmospheric perturbation spectra.

Year	2004	2004	2004	2004	2004	2005
Months	9–11	9–11	9–11	9–11	9–11	1
z, km	30	35	40	45	30–45	30
Latitudes, DEG	20° S–20° N	20° S–20° N	20° S–20° N	20° S–20° N	20° S–20° N	34° S–36° N
n	594	596	597	587	2374	147
$C_W, 10^{-11}\,\mathrm{m}^{-2}$	3–8	3–8	2–9	2–9	2–11	2–8
$C_K \sim a(C_W)^\gamma$						
r	0.24	0.37	0.32	0.36	0.44	0.49
a	2.05×10^{-4}	5.17×10^{-4}	48.7	0.068	55.1	0.69
γ	0.47	0.50	0.97	0.72	1.00	0.87
$k_0 \sim a(C_W)^\gamma$						
r		0.13	0.33	0.38	0.15	
a		50.0	1.10E6	61.6	0.39	
γ		0.42	0.85	0.45	0.22	
$k_W \sim a(C_W)^\gamma$						
r	−0.36		−0.20	−0.20	−0.25	−0.45
a	8.12		7.48×10^{-3}	5.18×10^{-3}	1.26×10^{-4}	1.74×10^{-3}
γ	−0.35		−0.14	−0.13	−0.32	−0.23

values of L_T, ε, and K, which are consistent with the average turbulent characteristics for January 2005 presented in Table 1 (see above).

Gurvich and Chunchuzov (2003) estimated parameters of anisotropic (Eq. 2) and isotropic (Eq. 4) spectra at altitudes of 25–70 km from measurements of stellar scintillations performed on-board the space stations Mir and Salyut. They found a systematic decrease in average k_W from 0.5 to 0.1 m^{-1} and an increase in C_K from 10^{-9} to 10^{-8} m$^{-2/3}$, when altitude changed from 30 to 50 km. This is generally consistent with the behavior of k_W and C_K at different altitudes between 30 and 45 km in Table 1 for September–November 2004. The parameter C_W of anisotropic spectrum obtained by Gurvich and Chunchuzov (2003) is less variable in height and $C_W \sim (5\text{--}7) \times 10^{-11}$ m^{-2} with a maximum at altitudes of about 40 km, which is similar to C_W behavior in Table 1. Gurvich and Kan (2003b) estimated turbulent kinetic energy dissipation rates using k_W from the same observations on-board the space stations Salyut and Mir. Their average ε increased with height from 10^{-6} to 5×10^{-5} W kg^{-1} between altitudes of 30 and 50 km. Values ε_i in Table 1 generally correspond to this behavior. Differences in exact values of mentioned parameters and characteristics in Table 1 and those estimated by Gurvich and Chunchuzov (2003) and Gurvich and Kan (2003b) might arise from the differences in years, seasons, latitudes and longitudes of observations with GOMOS and the space stations Salyut and Mir.

Correlations between parameters of anisotropic and isotropic perturbation spectra considered in Sect. 3.3 can be partly due to procedures of GOMOS data processing. For example, parameters C_W, k_0, k_W are calculated simultaneously and could have relations through mathematical expressions. On the other hand, there are physical reasons for observed correlations between parameters of anisotropic and isotropic spectra. One of the sources of turbulence in the middle atmosphere could be breaking IGWs (Lindzen, 1981; Fritts and Alexander, 2003). This could explain the positive correlation between parameters C_W and C_K in Table 2 and Fig. 5. It is usually supposed that anisotropic spectra (Eqs. 2 and 3) are mainly composed of saturated IGWs (Fritts and Alexander, 2003; Sofieva et al., 2007, 2010). Larger C_W can cause more intensive breaking of these IGWs and can produce larger amplitudes C_K of isotropic spectra of small-scale turbulence. Increased turbulence generated by stronger IGWs could produce stronger dissipation of shorter vertical scale waves or reduce their amplitudes through neutralization of the stable stratification and thus decrease the cutoff wavenumber of anisotropic spectrum k_W (see negative correlation between C_W and k_W in Table 2).

In Fig. 4, distributions of K_W at different altitudes in low latitudes have maxima concentrated at longitudes close to locations where maxima of IGW intensity and potential energy at altitudes of 15–25 km in the stratosphere were obtained with low-orbit GPS satellite measurements (Gavrilov, 2007; Alexander et al., 2008; Wang and Alexander, 2010). Similar maxima exist in the results of satellite measurements with microwave (MLS) and infrared limb instruments (e.g., Jiang et al., 2004; Ern et al., 2011; Ern and Preusse, 2012).
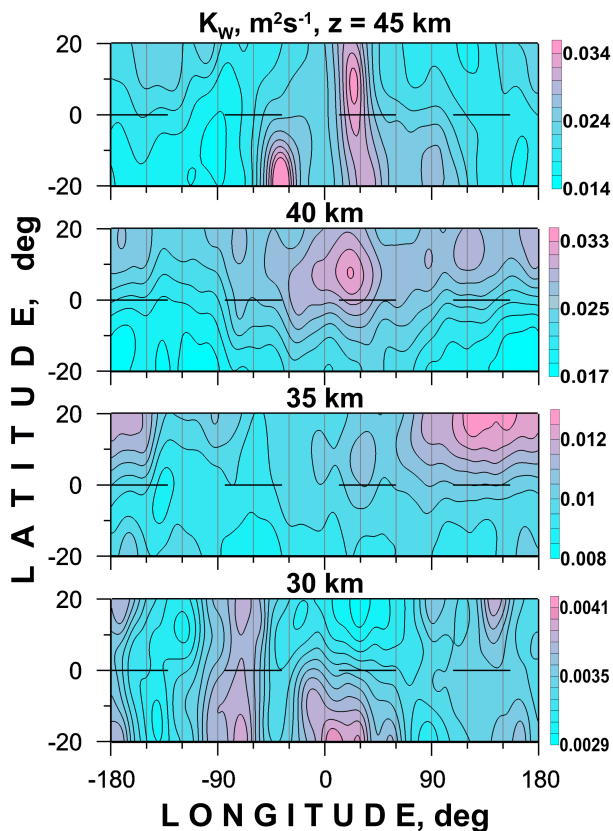
Fig. 4. Latitude-longitude distributions of turbulent diffusivity estimate K_W in September–November 2004 at different altitudes.
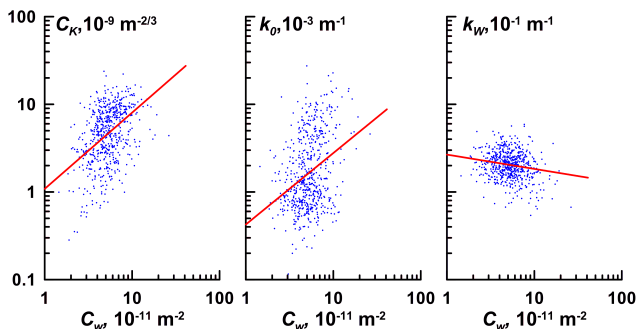

Fig. 5. Scatter plots for pairs of the spectral parameters presented in Table 2 for September–November 2004 at 40 km altitude.

This could confirm hypotheses about turbulence generation by breaking IGWs, which can propagate to the middle atmosphere from tropospheric orographic and convection wave sources. Gurvich et al. (2007) presented latitude-longitude distributions of the structure characteristic of the temperature field C_T^2 obtained from GOMOS observations for January–March and June–September 2003 at 42 km altitude. At low latitudes, they obtained C_T^2 maxima at the same longitude ranges, where the maxima of K_W are concentrated in Fig. 4.

Variability of latitude-longitude distributions of turbulent characteristics in Fig. 4 may show that interactions between anisotropic IGWs and isotropic turbulent spectra could be complicated. For example, dissipation inside intensive turbulent zones can suppress amplitudes of propagating wave spectral components. Therefore, above intensive turbulent zones, spectra of upward propagating IGWs may become weaker than those spectra above laminar layers. The latter become unstable and can generate turbulence there. Such interactions between IGW and turbulent spectra could produce interspersed locations of intensive IGWs and turbulence at different altitudes. Additional variability may arise from using values of Brunt–Vaisala frequency from meteorological models during processing the GOMOS data.

In this paper, we used three approaches to estimate the Thorpe scales from Eqs. (10), (12) and (13), namely $L_T = L_{Tb}$, L_{TW}, L_{Te}, and respective values of turbulent energy dissipation rates $\varepsilon_b, \varepsilon_W, \varepsilon_e$ and turbulent diffusivities K_b, K_W, K_e. These estimates utilize different sets of spectral parameters: C_W, C_K for L_{Tb}; C_K, k_W for for L_{TW}, and just C_K for L_{Te}. Table 1 shows that L_{Tb}, ε_b, K_b are usually smaller than respective L_{TW}, ε_W, K_W. This is the result of generally larger buoyancy wavenumbers k_b compared to k_W (see Fig. 1). As was mentioned in Sect. 3.2, differences between considered estimates of turbulent characteristics are usually not large, and one can use any of these approaches depending on available sets of anisotropic and isotropic spectral scales.

5   Conclusions

In this paper, we developed approaches for estimations of effective turbulent diffusion and energetic parameters from characteristics of anisotropic and isotropic spectra of perturbations of atmospheric refractivity, density and temperature. We use required spectral parameters from GOMOS satellite measurements of stellar scintillations to estimate turbulent Thorpe scales, L_T, diffusivities, K, and energy dissipation rates, ε, in the stratosphere. At low latitudes, average effective values for altitudes of 30–45 km in September–November 2004 are $L_T \sim 1$–1.1 m, $\varepsilon \sim (1.8$–$2.4) \times 10^{-5} \, \mathrm{W \, kg^{-1}}$, and $K \sim (1.2$–$1.6) \times 10^{-2} \, \mathrm{m^2 \, s^{-1}}$ depending on different sets of used parameters. Respective standard deviations of individual values due to all kinds of variability are $\delta L_T \sim 0.6$–0.7 m, $\delta \varepsilon \sim (2.3$–$3.5) \times 10^{-5} \, \mathrm{W \, kg^{-1}}$, and $\delta K \sim (1.7$–$2.6) \times 10^{-2} \, \mathrm{m^2 \, s^{-1}}$. These values correspond to high-resolution balloon measurements of turbulent characteristics in the stratosphere, and to previous satellite stellar scintillation measurements. At latitudes 20° S–20° N, distributions of turbulent characteristics have maxima at longitudes, which correspond to regions of increased gravity wave dissipation over continents and locations of stronger convection. Largest positive correlations exist between parameters C_W and C_K. Smaller

positive correlations may exist between C_W and k_0, also negative correlation between C_W and k_W.

Edited by: P. Haynes

References

Alexander, M. J., Tsuda, T., and Vincent, R. A.: Latitudinal variations observed in gravity waves with short vertical wavelengths, J. Atmos. Sci., 59, 1394–1404, 2002.

Alexander, M. J., Geller, M., McLandress, C., Polavarapu, S., Preusse, P., Sassi, F., Sato, K., Eckermann, S., Ern, M., Hertzog, A., Kawatani, Y. A., Pulido, M., Shaw, T., Sigmond, M., Vincent, R., and Watanabe, S.: Recent developments in gravity-wave effects in climate models and the global distribution of gravity-wave momentum flux from observations and models, Q. J. Roy. Meteorol. Soc. 136, 1103–1124, doi:10.1002/qj.637, 2010.

Alexander, S. P., Tsuda, T., Kawatani, Y., and Takahashi, M.: Global distribution of atmospheric waves in the equatorial upper troposphere and lower stratosphere: COSMIC observations of wave mean flow interactions, J. Geophys. Res., 113, D24115, doi:10.1029/2008JD010039, 2008.

Alisse, J. R.: Turbulence en atmosphere stable, Une etude quantitative, These de doctorat, Univ. Paris VI, 1999.

Bertaux, J. L., Kyrola, E., Fussen, D., Hauchecorne, A., Dalaudier, F., Sofieva, V., Tamminen, J., Vanhellemont, F., Fanton d'Andon, O., Barrot, G., Mangin, A., Blanot, L., Lebrun, J. C., Perot, K., Fehr, T., Saavedra, L., Leppelmeier, G. W., Fraisse, R.: Global ozone monitoring by occultation of stars: an overview of GOMOS measurements on ENVISAT, Atmos. Chem. Phys., 10, 12091–12148, doi:10.5194/acp-10-12091-2010, 2010.

Caldwell, D. R.: Oceanic turbulence: big bangs or continuous creation?, J. Geophys. Res., 88, 7543–7550, 1983.

Clayson, C. A., Kantha, L.: On turbulence and mixing in the free atmosphere inferred from high-resolution soundings, J. Atmos. Ocean. Technol., 25, 833–851, 2008.

Eckermann, S. and Preusse, P.: Global measurements of stratospheric mountain waves from space, Science, 286, 1534-1537, 1999.

Ern, M. and Preusse, P.: Gravity wave momentum flux spectra observed from satellite in the summertime subtropics: Implications for global modeling, Geophys. Res. Letters, 39, L15810, doi:10.1029/2012GL052659, 2012.

Ern, M., Preusse, P., Alexander, M. J., and Warner, C. D.: Absolute values of gravity wave momentum flux derived from satellite data, J. Geophys. Res., 109, D20103, doi:10.1029/2004JD004752, 2004.

Ern, M., Preusse, P., Gille, J. C., Hepplewhite, C. L., Mlynczak, M. G., Russell III, J. M., and Riese M.: Implications for atmospheric dynamics derived from global observations of gravity wave momentum flux in stratosphere and mesosphere, J. Geophys. Res., 116, D19107, doi:10.1029/2011JD015821, 2011.

Fer, I., Skogseth, R., and Haugan, P. M.: Mixing of the Storjorden overflow (Svalbard Archipelago) inferred from density overturns, J. Geophys. Res., 109, 1–14, 2004.

Fetzer, E. J. and Gille, J. C.: Gravity wave variance in LIMS temperatures. Part I: Variability and comparison with background winds, J. Atmos. Sci., 51, 2461–2483, 1994.

Fritts, D. C. and Alexander, M. J.: Gravity wave dynamics and effects in the middle atmosphere, Rev. Geophys. 41, 1003, doi:10.1029/2001RG000106, 2003.

Fukao, S., Yamanaka, M. D., Ao, N., Hocking, W. K., Sato, T., Yamamoto, M., Nakamura, T., Tsuda, T., and Kato, S.: Seasonal variability of vertical eddy diffusivity in the middle atmosphere, 1. Three-year observations by the middle and upper atmosphere radar, J. Geophys. Res., 99, 18973–18987, 1994.

Galbraith, P. S. and Kelley, D. E.: Identifying overturns in CTD profiles, J. Atmos. Ocean. Technol., 13, 688–702, 1996.

Gavrilov, N. M.: Structure of the mesoscale variability of the troposphere and stratosphere found from radio refraction measurements via CHAMP satellite, Izvestiya, Atmos. Ocean. Phys., 43, 451–460, 2007.

Gavrilov, N. M. and Karpova, N. V.: Global structure of mesoscale variability of the atmosphere from satellite measurements of radio wave refraction, Izvestia, Atmos. Ocean. Phys., 40, 747–758, 2004.

Gavrilov, N. M., Karpova, N. V., Jacobi, Ch., and Gavrilov, A. N.: Morphology of atmospheric refraction index variations at different altitudes from GPS/MET satellite observations, J. Atmos. Sol.-Terr. Phys., 66, 427–435, 2004.

Gavrilov, N. M., Luce, H., Crochet, M., Dalaudier, F., and Fukao, S.: Turbulence parameter estimations from high-resolution balloon temperature measurements of the MUTSI-2000 campaign, Ann. Geophys., 23, 2401–2413, doi:10.5194/angeo-23-2401-2005, 2005.

Gurvich, A. S. and Brekhovskikh, V. L.: Study of the turbulence and inner waves in the stratosphere based on the observations of stellar scintillations from space: A model of scintillation spectra, Waves Random Media, 11, 163–181, 2001.

Gurvich, A. S. and Chunchuzov, I. P.: Parameters of the fine density structure in the stratosphere obtained from spacecraft observations of stellar scintillations, J. Geophys. Res., 108, 4166, doi:10.1029/2002JD002281, 2003.

Gurvich, A. S. and Kan V.: Structure of air density irregularities in the stratosphere from spacecraft observations of stellar scintillation: 1. Three-dimensional spectrum model and recovery of its parameters, Izvestia, Atmos. Ocean. Phys., 39, 300–310, 2003a.

Gurvich, A. S. and Kan V.: Structure of air density irregularities in the stratosphere from spacecraft observations of stellar scintillation: 2. Characteristic scales, structure characteristics, and kinetic energy dissipation, Izvestiya, Atmos. Ocean. Phys., 39, 311–321, 2003b.

Gurvich, A. S., Kan, V., Savchenko, S. A., Pakhomov, A. I., Padalka, G. I.: Studying the turbulence and internal waves in the stratosphere from spacecraft observations of stellar scintillation: II. Probability distributions and scintillation spectra, Izvestia, Atmos. Ocean. Phys., 37, 452–465, 2001.

Gurvich, A. S., Sofieva, V. F., and Dalaudier, F.: Global distribution of CT^2 at altitudes 30–50 km from space-borne observations of stellar scintillation. Geophys. Res. Lett., 34, L24813, doi:10.1029/2007GL031134, 2007.

Jiang, J. H., Wang, B., Goya, K., Hocke, K., Eckermann, S. D., Ma, J., Wu, D. L., and Read, W. J.: Geographical distribution and interseasonal variability of tropical deep convection: UARS MLS observations and analyses, J. Geophys. Res., 109, D03111, doi:10.1029/2003JD003756, 2004.

Lindzen, R. S.: Turbulence and Stress Owing to Gravity Wave and Tidal Breakdown, J. Geophys. Res., 86, 9707–9714, 1981.

Lumley, J. L.: The spectrum of nearly inertial turbulence in a stably stratified fluid, J. Atmos. Sci., 21, 99–102, 1964.

McLandress, C., Alexander, M. J., and Wu, D.: Microwave limb sounder observations of gravity waves in the stratosphere: A climatology and interpretation, J. Geophys. Res., 105, 11947–11967, 2000.

Monin, A. S. and Yaglom, A. M.: Statistical Fluid Mechanics, vol. 2, MIT Press, Cambridge, Mass., 1975.

Ottersten H.: Atmospheric structure and radar backscattering in clear air, Radio Sci., 4, 1179–1193, 1969.

Press, W. H., Teukolsky, S. A., Vetterling, W. T., Flannery, B. P.: Numerical Recipes in FORTRAN, The Art of Scientific Computing, Oxford, Clarendon, 1992.

Schmidt, T., de la Torre, A., and Wickert, J.: Global gravity wave activity in the tropopause region from CHAMP radio occultation data, Geophys. Res. Lett., 35, L16807, doi:10.1029/2008GL034986, 2008.

Smith, S. A., Fritts, D. C., and VanZandt, T. E.: Evidence of a saturation spectrum of atmospheric gravity waves, J. Atmos. Sci., 44, 1404–1410, 1987.

Sofieva, V. F., Gurvich, A. S., Dalaudier, F., and Kan, V.: Reconstruction of internal gravity wave and turbulence parameters in the stratosphere using GOMOS scintillation measurements, J. Geophys. Res., 112, D12113, doi:10.1029/2006JD007483, 2007.

Sofieva, V. F., Gurvich, A. S., and Dalaudier, F.: Gravity wave spectra parameters in 2003 retrieved from stellar scintillation measurements by GOMOS, Geophys. Res. Lett., 36, L05811, doi:10.1029/2008GL036726, 2009.

Sofieva, V. F., Gurvich, A. S., and Dalaudier, F.: Mapping gravity waves and turbulence in the stratosphere using satellite measurements of stellar scintillation, Physica Scripta, T142, 014043, doi:10.1088/0031-8949/2010/T142/014043, 2010.

Tatarskii, V. I.: The Effects of the Turbulent Atmosphere on Wave Propagation, US Dep. of Commer., Washington, DC, 1971.

Tsuda, T., Nishida, M., Rocken, C., and Ware, R. H.: A global morphology of gravity wave activity in the stratosphere revealed by the GPS occultation data (GPS/MET), J. Geophys. Res., 105, 7257–7274, 2000.

Wang, L. and Alexander, M. J.: Global estimates of gravity wave parameters from GPS radio occultation temperature data, J. Geophys. Res., 115, D21122, doi:10.1029/2010JD013860, 2010.

Wu, D. and Waters, J.: Gravity-wave-scale temperature fluctuations seen by the UARS MLS, Geophys. Res. Lett., 23, 3289–3292, 1996.

Wu, D. L., Preusse, P., Eckermann, S. D., Jiang, J. H., de la Torre, J. M., Coy, L., Lawrence, B., and Wang, D. Y.: Remote sounding of atmospheric gravity waves with satellite limb and nadir techniques, Adv. Space Res., 37, 2269–2277, 2006.